Supramolecular Chemistry
Publication details, including instructions for authors and subscription information:
http://www.informaworld.com/smpp/title~content=t713649759

Platinum group metal thiacrown complexes as precursors for self-assembly reactions

Gregory J. Grant[a]; Rishi D. Naik[a]; Daron E. Janzen[a]; Desirée A. Benefield[a]; Donald G. VanDerveer[b]
[a] Department of Chemistry, University of Tennessee, Chattanooga, TN, USA [b] School of Chemistry, Clemson University, Clemson, SC, USA

Online publication date: 18 January 2010

To cite this Article Grant, Gregory J. , Naik, Rishi D. , Janzen, Daron E. , Benefield, Desirée A. and VanDerveer, Donald G.(2010) 'Platinum group metal thiacrown complexes as precursors for self-assembly reactions', Supramolecular Chemistry, 22: 2, 109 — 121
To link to this Article: DOI: 10.1080/10610270903304426
URL: http://dx.doi.org/10.1080/10610270903304426

Supramolecular Chemistry
Vol. 22, No. 2, February 2010, 109–121

Taylor & Francis
Taylor & Francis Group

Platinum group metal thiacrown complexes as precursors for self-assembly reactions

Gregory J. Grant[a]*, Rishi D. Naik[a], Daron E. Janzen[a†], Desirée A. Benefield[a] and Donald G. VanDerveer[b]

[a]*Department of Chemistry, University of Tennessee, Chattanooga, TN 37403, USA;* [b]*School of Chemistry, Clemson University, Clemson, SC, USA*

(*Received 9 July 2009; final version received 30 August 2009*)

We report that our previously published molecular square, $[\{Pt([9]aneS_3)(bipy)\}_4](OTf)_8$, although quite stable in nitromethane, slowly establishes an equilibrium with another coordination polymer, most likely a triangle, in acetonitrile. Multinuclear measurements on the square precursor complex, $[Pt([9]aneS_3)Cl_2]$, show acetonitrile coordination upon dechlorination in that solvent, and acetonitrile coordination is additionally confirmed by the solid-state structure of $[Pt([9]aneS_3)(MeCN)_2]^{2+}$. We form the complex through the reaction of $[Pt([9]aneS_3)Cl_2]$ with excess $AgPF_6$ in refluxing MeCN to produce a solid-state solution containing two complex cations with exclusive hexafluorophosphate counterions. Besides $[Pt([9]aneS_3)(MeCN)_2]^{2+}$, a second cation is obtained, $[Pt([9]aneS_3)_2]^{2+}$, which shows disorder between a double *endo* and a rare double *exo* conformation for the two $[9]aneS_3$ ligands. We also report the structures of two Rh(III) thiacrown complexes, *cis*-$[Rh([12]aneS_4)Cl_2](PF_6)$, which involves *cis* chloro ligands and an asymmetric binding of the two equatorial sulphur donors, as well as *trans*-$[Rh([16]aneS_4)(H_2O)(Cl)](OTf)_2$ with adjacent rather than alternating chair and twist-boat conformations. Lastly, the crystal structure of $[\{Pd([9]aneS_3)(Cl)\}_2(pyrazine)](OTf)_2$ displays a pyrazine ligand bridging two $[Pd([9]aneS_3)Cl]^+$ moieties with *cis* stereochemistry of the two chloro ligands. Distortion of the pyrazine ligand is observed, which alleviates strain from bridging the two Pd centres. The extended structure of the complex consists of chains of dimers running parallel to the *b*-axis of the crystal.

Keywords: thiacrown complexes; self-assembly; supramolecular complexes; crystal structures; molecular squares

1. Introduction

Metal-directed self-assembly of molecular squares was pioneered in the 1990s by the Fujita and Stang research groups through the use of Pd(II) and Pt(II) complexes, employing diamine and diphosphine capping ligands, respectively (*1*, *2*). Since that time, the field of metallosupramolecular chemistry has grown substantially and emerged as an important area of research with these solid materials being used in an impressive array of applications including artificial molecular machines (*3–5*), storage of hydrogen, methane and other strategic gases (*6*, *7*), gas adsorption (*8*, *9*), solvent inclusion (*10*, *11*), heterogeneous catalysis (*12*, *13*) and electronic properties (*14*). Many excellent reviews dealing with transition metal coordination polymers formed by self-assembly have now appeared (*15–25*), and the enhanced ability to perform single-crystal structural determinations of the molecules with greater ease and efficiency has certainly played a pivotal role in the evolution of the field. An impressive and elegant collection of 2D and 3D structures involving transition metal complexes as vertices linked by linear bidentate bridging ligands such as pyrazine and 4,4′-bipyridine has been reported. A very recent review has appeared, which is devoted exclusively to trinuclear metallacycles including molecular triangles formed by self-assembly processes (*26*).

Long and co-workers noted that ruthenium(II) complexes containing capping ligands such as the tetraaza macrocycle, $[12]aneN_4$, could be utilised as vertices for the preparation of both molecular squares and triangles (*27*, *28*). Our group and others have been interested in extending this chemistry to incorporate macrocyclic thioether ligands into metallosupramolecular structures (*29–31*). Mononuclear platinum group metal complexes containing thiacrown ligands such as $[9]aneS_3$ (1,4,7-trithiacyclononane) show interesting physicochemical properties including surprisingly large ligand field splittings, the formation of unusual coordination geometries and the stabilisation of rare oxidation states such as Pd(III) and Rh(II) (*32–35*). We have reported a molecular square containing Pt/$[9]aneS_3$ corners, which direct the self-assembly of 4,4′-bipyridine linkers into a molecular square (*29*). The square maintains the fluxionality of all four $[9]aneS_3$ macrocycles (observed in the mononuclear complex), resulting in a single ^{13}C NMR resonance for the 24 methylene carbons. Triangles using Ru/$[9]aneS_3$ vertices have also been reported by both

*Corresponding author. Email: greg-grant@utc.edu

†Present address: Department of Chemistry, College of St Catherine, St Paul, MN, USA.

ISSN 1061-0278 print/ISSN 1029-0478 online

DOI: 10.1080/10610270903304426
http://www.informaworld.com

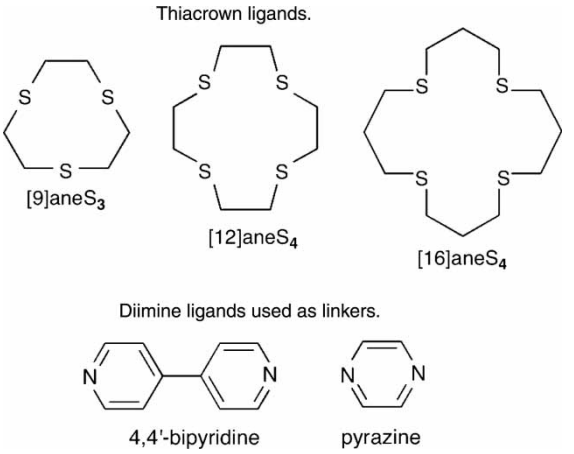

Scheme 1. Ligands used in this study.

the Alessio and Thomas groups (*30*, *31*). Silver dechlorination methods are typically employed prior to self-assembly for removal of halide ligands in the vertex metal complex. There can be difficulties in the removal of chloride ion, particularly for highly inert metal ions such as Rh(III) and Ir(III), which is a prerequisite for self-assembly into supramolecular structures. Our group is interested in exploring dechlorination using triflic acid as an alternative synthetic tool since this reagent had been successively used in a similar manner for other transition metal complexes (*36*, *37*). We also report the synthesis of several platinum group metal complexes containing thiacrown ligands, which are potential vertices for metal-directed self-assembly into supramolecular structures. The thiacrown and diimine linker ligands examined in this study are shown in Scheme 1.

2. Experimental

2.1 Materials

All commercial solvents, ligands and other reagents were used as received. The starting metal complexes, $[Pd([9]aneS_3)Cl_2]$, $[Pt([9]aneS_3)Cl_2]$ (*38*), $[Rh([12]aneS_4)Cl_2](PF_6)$ (*39*), $[Rh([9]aneS_3)Cl_3]$ and $[Ir([9]aneS_3)Cl_3]$ (*40*), were prepared by the published methods. ***Caution!*** *Triflic acid is one of the strongest acids known and is extremely corrosive* (*36*, *37*). *It is necessary to take safety precautions to prevent contact with skin and eyes during the reaction. HCl gas is rapidly evolved in this reaction. Reactions with triflic acid should be only used in a well-functioning fume hood, and all waste solutions containing the compound should be carefully neutralised with 0.1 M NaOH.*

2.2 Measurements

Elemental analyses were performed by Atlantic Microlab, Inc. of Atlanta, Georgia. Fourier transform IR spectra were obtained as KBr powders using pre-weighed 500 mg packets and a Nicolet Impact 410 spectrometer equipped with an ATR accessory. UV–vis spectra were obtained in acetonitrile using a Varian DMS 200 UV–visible spectrophotometer. All $^{13}C\{^1H\}$, $^{195}Pt\{^1H\}$, ^{19}F and ^1H NMR spectra were recorded on either a JEOL ECX-400 NMR spectrometer or a Varian Gemini 2000 300 MHz NMR spectrometer using residual solvent peaks for both the deuterium lock and internal reference except for $^{195}Pt\{^1H\}$ NMR spectra which were referenced externally to $[PtCl_4]^{2-}$ at -1624 ppm (*41*).

2.3 Synthetic procedures, mononuclear complexes

2.3.1 $[Pt([9]aneS_3)(OTf)_2]$ (1)

The reaction proceeds under nitrogen with stirring. A nitrogen-purged flask is charged with an orange crystalline sample of $[Pt([9]aneS_3)Cl_2]$ weighing 1.18 g (2.65 mmol). A 5.0 g mass of triflic acid (33 mmol) is transferred via a syringe to a pressure-equalised dropping funnel and slowly added dropwise. The reaction is indicated by the loss of the orange solid and formation of a red-brown solution. The presence of HCl gas is confirmed by bubbling the exiting gas into an aqueous silver nitrate solution. After 2.5 h, no more AgCl is formed. Very slowly, small portions of diethyl ether (3×25 ml) are added to the red-brown oil. A red-brown microcrystalline solid forms immediately. This solid is removed by filtration, washed with diethyl ether (3×50 ml) and air-dried to yield 1.790 g (2.389 mmol, 90.2% yield) $[Pt([9]aneS_3)(H_2O)_2](OTf)_2$ as a brick red powder. The compound is hygroscopic, turning into a dark sticky oil upon prolonged exposure to air. Anal. calcd for $C_8H_{22}F_6O_8P_2PtS_6$: C, 13.43; H, 3.10. Found: C, 13.77; H, 3.16. δ_H (400 MHz, CD_3NO_2): broad singlet at 8.81 ppm (coordinated *H_2O*, 4H), broad, complex, poorly resolved pattern at 4.2–3.0 ppm (*[9]aneS*$_3$, 6H). δ_C (100 MHz, CD_3NO_2): quartet centred at 121.98 ppm ($^1J_{F-C} = 68$ Hz, *OTf^-*), complex peak pattern at 42.7–34.6 ppm (*[9]aneS*$_3$). δ_F (376 MHz, CD_3NO_2): -79.54 ppm (br s, *OTf^-*). δ_{Pt} (86 MHz, CD_3NO_2): -4848 ppm ($\nu_{1/2} = 100$ Hz).

2.3.2 $[Pt([9]aneS_3)(MeCN)_2]_2[Pt([9]aneS_3)_2](PF_6)_6$ (2)

A 1:3 mixture of $[Pt([9]aneS_3)Cl_2]$ (50.0 mg, 0.112 mmol) and $AgPF_6$ (86.4 mg, 0.336 mmol) is refluxed in 10 ml of acetonitrile for 2.5 h. The anticipated mass of AgCl (32 mg) is removed by filtration. The solution is concentrated to one-third of its original volume and diethyl ether is diffused into the orange solution over several days to yield X-ray quality crystals of $[Pt([9]aneS_3)(MeCN)_2]_2[Pt([9]aneS_3)_2](PF_6)_6$. We have also studied the NMR behaviour of $[Pt([9]aneS_3)(OTf)_2]$ (**1**) in CD_3CN. δ_H (400 MHz, CD_3CN): AA′BB′ multiplets

at 3.29–3.16 ppm (6H, *[9]aneS$_3$*) and 3.11–2.98 ppm (6H, *[9]aneS$_3$*). δ_C (100 MHz, CD_3CN): 36.62 ppm (*[9]aneS$_3$*). δ_F (376 MHz, CD_3CN): −79.22 ppm (*OTf$^-$*).

2.3.3 *cis-[Rh([12]aneS$_4$)Cl$_2$](PF$_6$) (**3**)*

The compound was prepared by the literature method in a 94.2% yield (*39*). Formation of the complex is confirmed through its ^{13}C NMR spectrum which matches the reported literature values. δ_C (100 MHz, CD_3NO_2): 46.53, 43.16, 38.17, 37.27 ppm. Diffusion of ether into a concentrated acetonitrile solution produced X-ray quality crystals of **3**.

2.3.4 *trans-[Rh([16]aneS$_4$)(H$_2$O)(Cl)](OTf)$_2$ (**4**)*

The complex *trans*-[Rh([16]aneS$_4$)Cl$_2$]Cl is prepared in 95.25% yield using the literature method described for the preparation of [Rh([16]aneS$_4$)Cl$_2$](PF$_6$) (*39*). The formation of the desired product is confirmed by its ^{13}C NMR spectrum. A full description of the synthesis of the chloride salt appears in the Supplementary Information.

The reaction of *trans*-[Rh([16]aneS$_4$)Cl$_2$]Cl with triflic acid proceeds under nitrogen and with stirring using the procedure described for compound **1**. A mass weighing 491 mg (0.971 mmol) of [Rh([16]aneS$_4$)Cl$_2$]Cl as a bright orange solid is reacted with 5.0 g of triflic acid (33 mmol). After 5 h, no additional HCl is generated from the reaction. At that time, 25 ml of diethyl ether was added slowly to the orange solution, resulting in the precipitation of an orange solid. The solid was filtered, washed with diethyl ether (3 × 25 ml) and air-dried to yield 523 mg (71.7%) of crude *trans*-[Rh([16]aneS$_4$)(H$_2$O)(Cl)](OTf)$_2$ as an orange crystalline solid. ν_{max} (cm^{-1}): 3000 (broad, OH), 2972, 2924 (C—H), 1620 (broad, OH), 1430, 1310, 1268 (OTf$^-$), 1152 (OTf$^-$), 1025 (OTf$^-$), 879, 660 (C—S), 637 (OTf$^-$), 572, 516. The compound was dissolved in nitromethane, and diethyl ether slowly diffused into the orange-yellow solution forming two crystalline products, yellow needles and amber plates. The two crystalline forms were mechanically separated. The yellow needles were confirmed via chemical analysis and ^{13}C NMR spectroscopy to be *trans*-[Rh([16]aneS$_4$)(H$_2$O)(Cl)](OTf)$_2$. The amber plates were analysed by single-crystal X-ray diffraction and are also shown to be *trans*-[Rh([16]aneS$_4$)(H$_2$O)(Cl)](OTf)$_2$. δ_H (400 MHz, CD_3NO_2): complex multiplets at 3.4–2.6 ppm (—S—C*H$_2$*—*CH$_2$*—*CH$_2$*—S—) and 2.3–2.2 ppm (—S—CH$_2$—C*H$_2$*—*CH$_2$*—*S*—). δ_C (100 MHz, CD_3NO_2): singlet at 126.21 ppm (uncomplexed *OTf$^-$*), quartet centred at 122.25 ppm (complexed *OTf$^-$*, $^1J_{CF} = 320$ Hz), complex pattern at 37.50–32.63 ppm (—S—*C*H$_2$—CH$_2$—*C*H$_2$—S—) and complex pattern at 24.92–23.41 ppm (—S—CH$_2$—*C*H$_2$—CH$_2$—S—). δ_F (376 MHz, CD_3NO_2): singlets at −79.10 ppm (*OTf$^-$*) and −79.62 ppm (*OTf$^-$*). A portion of *trans*-[Rh([16]aneS$_4$)(H$_2$O)(Cl)](OTf)$_2$ was recrystallised from MeCN–diethyl ether for chemical analysis. In MeCN solvent, the water is displaced by the acetonitrile to form [Rh([16]aneS$_4$)(CH$_3$CN)(Cl)](OTf)$_2$. Anal. calcd for $C_{16}H_{27}ClF_6NO_6RhS_6$: C, 24.85; H, 3.52; N, 1.81. Found: C, 24.99; H, 3.54; N, 1.70.

2.4 *Synthetic procedures, binuclear and polynuclear complexes*

2.4.1 *[{Pt([9]aneS$_3$)(Cl)}$_2$(bipy)](PF$_6$)$_2$ (**5**)*

A mixture of [Pt([9]aneS$_3$)Cl$_2$] (100 mg, 0.224 mmol) and $AgPF_6$ (56.6 mg, 0.224 mmol) was stirred in 10 ml of CH_3CN for 24 h. A quantitative amount of AgCl (31 mg) was removed as a white precipitate. A mass of 4,4′-bipyridine (17.5 mg, 0.112 mmol) was added to the solution, which was then stirred for 6 days. The solution was concentrated to one-third of its original volume, and diethyl ether was slowly diffused into it to produce orange needles of [{Pt([9]aneS$_3$)(Cl)}$_2$(bipy)](PF$_6$)$_2$ (128 mg, 90.0%). Anal. calcd for $C_{22}Cl_2H_{32}F_{12}N_2P_2Pt_2S_6$: C, 20.84; Cl, 5.59; H, 2.54; N, 2.21; S, 15.17. Found: C, 20.85; Cl, 5.56; H, 2.82; N, 2.37; S, 14.83. δ_H (300 MHz, CD_3NO_2): 9.09 (d, 4H, *4,4′-bipy*), 7.98 (d, 4H, *4,4′-bipy*), 3.37–3.21 (m, 24H, *[9]aneS$_3$*). δ_C (75 MHz, CD_3NO_2): 154.6 (4C, *4,4′-bipy*), 148.4 (2C, *4,4′-bipy*), 126.6 (4C, *4,4′-bipy*), 37.1 (12C, *[9]aneS$_3$*). δ_{Pt} (64 MHz, CD_3NO_2): −3343 ppm. ν_{max} (cm^{-1}): 3096.6, 3048.3, 2965.5, 1606.9, 1524.1, 1482.8, 1406.9, 1282.8, 1227.6, 1062.1, 931.0, 841.4 (s, PF$_6$), 655.5 (m, C–S), 551.7 (s, PF$_6^-$). UV–vis (CH_3CN, nm (ε, M^{-1} cm^{-1})): 273(5200).

2.4.2 *Preparation of cis-[{Pd([9]aneS$_3$)(Cl)}$_2$(pyrazine)](OTf)$_2$ (**6**)*

The starting complex [Pd([9]aneS$_3$)(H$_2$O)(Cl)](OTf) was prepared by a procedure similar to that used for compound **1**. A full description of the synthesis of the compound appears in the Supplementary Information. A mass of 43.8 mg of [Pd([9]aneS$_3$)(Cl)(H$_2$O)](OTf) (0.0895 mmol) is mixed with 6.00 mg of pyrazine (0.0750 mmol) in 25 ml of nitromethane and stirred for 24 h. At that time, a clear red-brown solution is present, which is concentrated to 0.8 ml. Diffusion of diethyl ether into the mixture forms X-ray quality crystals of [{Pd([9]aneS$_3$)(Cl)}$_2$(pyz)](OTf)$_2$. δ_H (400 MHz, CD_3CN): 8.83 ppm (d, *pyz*), 8.74 ppm (d, *pyz*), 3.41–3.24 and 3.19–3.02 ppm (m, *[9]aneS$_3$*). Evidence for the presence of a second pyrazine-linked complex is seen with a weaker set of equal intensity doublets at 8.92 and 8.69 ppm.

*2.4.3 Preparation and characterisation of [{Pt([9]aneS$_3$)(bipy)}$_4$](OTf)$_8$ (**7**) (molecular square)*

The synthesis of the compound has been previously reported, but we offer an improved chemical synthesis for the square as well as previously unpublished data (*29*). A mass of 99.2 mg [Pt([9]aneS$_3$)Cl$_2$] (0.226 mmol) is added to silver triflate, AgOTf (116 mg, 0.452 mmol) and refluxed in 10 ml of acetonitrile for 3.5 h. The solution is cooled to 0°C for several hours to precipitate a nearly quantitative amount of AgCl (64.2 mg). To ensure full separation from the AgCl, the yellow supernatant is removed two times from the solid by centrifugation. A mass of 38.4 mg (0.246 mmol) of 4,4′-bipyridine is added to the yellow supernatant and allowed to react for 6 days at room temperature. At that time, a small amount of residual AgCl is removed, and the solution is concentrated to one-third of its original volume resulting in a dark yellow slightly turbid solution. The solution is centrifuged again to remove any insoluble materials, and diethyl ether is slowly diffused into the bright yellow solution to yield a quantitative amount (191 mg) of yellow crystals of [{Pt([9]aneS$_3$)(bipy)}$_4$](OTf)$_8$. δ_H (400 MHz, CD_3CN) 8.98 ppm (d, 4H, *4,4′-bipy*), 7.89 (d, 4H, *4,4′-bipy*), 3.40–3.00 (m, 12H, *[9]aneS$_3$*). δ_C (100 MHz, CD_3CN) 158.22 ppm (4C, *4,4′-bipy*), 151.45 ppm (2C, *4,4′-bipy*), 130.99 ppm (4C, *4,4′-bipy*), 38.04 (6C, *[9]aneS$_3$*). δ_F (376 MHz, CD_3CN): −79.10 ppm ($\nu_{1/2} = 12$ Hz, OTf^-) ppm. With time, the square appears to degrade through the appearance of additional and new pair of doublets at 8.88 and 7.90 ppm (see Supplementary Information). The integration ratio of the former pair of doublets (molecular square) to the latter set is 79/21. The $^{13}C\{^1H\}$ NMR spectrum also shows similar behaviour. Besides the above resonances for **7**, the following resonances appear as a minor component: 157.99 ppm (4C, *4,4′-bipy*), 150.74 ppm (2C, *4,4′-bipy*), 130.49 ppm (4C, *4,4′-bipy*), 38.85 ppm (broad, $\nu_{1/2} = 12$ Hz, 6C, *[9]aneS$_3$*) (see Supplementary Information). The line width of the [9]aneS$_3$ resonances is too broad to resolve into separate individual components of the two species.

2.5 Crystallographic information on structures for compounds 2–4 and 6

*2.5.1 [Pt([9]aneS$_3$)(MeCN)$_2$]$_2$[Pt([9]aneS$_3$)$_2$](PF$_6$)$_6$ (**2**)*

A crystal (approximate dimensions $0.26 \times 0.15 \times 0.10\ mm^3$) was placed onto the tip of a 0.1 mm diameter glass capillary and mounted on a Rigaku AFC8S Mercury CCD diffractometer for data collection at 173(2) K. A preliminary set of cell constants was calculated from reflections harvested from a few frames. The data collection was carried out using Mo Kα radiation (graphite monochromator). The intensity data were corrected for absorption and decay (REQAB) (*42*). Final cell constants were calculated from the *xyz* centroids of 7614 strong reflections from the actual data collection after integration (CrystalClear) (*43*). Refer to Table 1 for additional crystal and refinement information. The structure was solved and refined using the SHELXTL software package (*44*). The space group *P-1* was determined based on systematic absences and intensity statistics. A direct methods solution was calculated, which provided most non-hydrogen atoms from the E-map. Full-matrix least-squares/difference Fourier cycles were performed, which located the remaining non-hydrogen atoms. All non-hydrogen atoms were refined with anisotropic displacement parameters. All hydrogen atoms were placed in ideal positions and refined as riding atoms with relative isotropic displacement parameters. The final full-matrix least-squares refinement converged to $R_1 = 0.0432$ and $wR_2 = 0.1130$ (F^2, all data).

The [9]aneS$_3$ ligand in [Pt([9]aneS$_3$)$_2$]$^{2+}$ adopts two different conformations, modelled as disorder, with both *endo* and *exo* coordinations of the [9]aneS$_3$ ligands. The disorder ratio is 77.0% *endodenate*/23.0% *exodentate*, and the S4, C11, C12, S5 strap of the [9]aneS$_3$ is not disordered. The [9]aneS$_3$ straps involving atoms C13, C14, S5, C15, C16 of the *endo* ligation and C13′, C14′, S5′, C15′, C16′ of the *exodentate* [9]aneS$_3$ ligation adopt different conformations. As the *exodentate* [9]aneS$_3$ ligand conformation is a disorder component as a part of the complex [Pt([9]aneS$_3$)$_2$]$^{2+}$, which has the Pt on a special position with inversion symmetry, this *exo* disorder component is required for both [9]aneS$_3$ ligands of the [Pt([9]aneS$_3$)$_2$]$^{2+}$ cation. Modest constraints were applied as a part of this refinement model. Atom pairs S6 and S6′, C14 and C14′, C15 and C15′, C13 and C13′, and C16 and C16′ were constrained to have identical thermal displacement parameters. Also, atom pairs S5 and S5′, S4 and S4′, and S5 and S5′ were constrained to have identical coordinates. A similarity restraint was applied between the following atoms in the two disorder components of the [9]aneS$_3$ ligand (S5, C13, C14, S6, C15, C16, S4 with the atoms S5′, C13′, C14′, S6′, C15′, C16′, S4′).

*2.5.2 [Rh([12]aneS$_4$)Cl$_2$](PF$_6$) (**3**)*

A crystal (approximate dimensions $0.24 \times 0.22 \times 0.22\ mm^3$) was placed onto the tip of a 0.1 mm diameter glass capillary and mounted on a Rigaku AFC8S Mercury CCD diffractometer for a data collection at 153(2) K. A preliminary set of cell constants was calculated from reflections harvested from a few frames. The data collection was carried out using Mo Kα radiation (graphite monochromator). The intensity data were corrected for absorption and decay (REQAB) (*42*). Final cell constants were calculated from the *xyz* centroids of 13,689 strong reflections from the actual data collection after integration

Table 1. Crystal data, data collection and refinement parameters for $[Pt([9]aneS_3)(MeCN)_2]_2[Pt([9]aneS_3)_2](PF_6)_6$ (**2**), $[Rh([12]aneS_4)Cl_2](PF_6)$ (**3**), *trans*-$[Rh([16]aneS_4)(H_2O)Cl)](OTf)_2$ (**4**) and $[\{Pd([9]aneS_3)(Cl)\}_2(pyrazine)](OTf)_2$ (**6**).

Compound	**2**	**3**	**4**	**6**
Formula	$C_{32}H_{60}F_{36}N_4P_6Pt_3S_{12}$	$C_8H_{16}Cl_2F_6PRhS_4$	$C_{14}H_{26}ClF_6N_2O_7RhS_6$	$C_{18}H_{28}Cl_2F_6N_2O_6PdS_8$
Habit, colour	Yellow, block	Orange, block	Orange, chip	Orange, chip
Lattice type	Triclinic	Monoclinic	Triclinic	Monoclinic
Space group	*P-1*	*P2₁/n*	*P-1*	*C2/m*
a (Å)	11.069 (2)	10.2435 (15)	10.682 (3)	16.407 (3)
b (Å)	11.233 (2)	23.159 (4)	11.5211 (6)	17.349 (4)
c (Å)	13.967 (3)	14.780 (2)	12.269 (3)	13.372 (2)
α (°)	87.21 (3)	90	71.49 (2)	90
β (°)	80.61 (3)	92.929 (6)	89.59 (3)	107.492 (5)
γ (°)	80.77 (3)	90	68.59 (2)	90
V (Å^3)	1690.6 (6)	3172.5 (11)	1322.9 (5)	3630.2 (12)
Z	1	8	2	4
Temperature (K)	173 (2)	153 (2)	153 (2)	158 (2)
Fwt. (g mol^{-1})	2340.65	559.23	751.07	908.90
D_c (Mg m^{-3})	2.299	2.122	1.886	1.871
μ (mm^{-1})	6.837	1.895	1.296	1.664
Reflections collected	15,788	27,615	10,120	14,499
Unique reflections	5964 [R(int) = 0.0465]	6765 [R(int) = 0.0513]	4607 [R(int) = 0.0474]	3335 [R(int) = 0.0265]
Max., min. transmission	0.5042, 0.1882	0.6602, 0.6391	0.9147, 0.7908	0.8253, 0.5705
Data, restraints, parameters	5964/12/439	6765/0/397	4607/3/6322	3335/0/127
R_1, wR_2 ($I > 2\sigma(I)$)	0.0432, 0.1069	0.0481, 0.0862	0.0525, 0.1233	0.0429, 0.1211
R_1, wR_2 (all data)	0.0533, 0.1130	0.0673, 0.0920	0.0784, 0.1550	0.0456, 0.1230
Goodness of fit (F^2)	1.070	1.190	1.074	1.114
Largest diff. peak, hole, (e Å^{-3})	3.886, −1.281	0.667, −0.800	0.992, −0.931	1.136, −0.576

(CrystalClear) (*43*). Refer to Table 1 for additional crystal and refinement information. The structure was solved and refined using the SHELXTL software package (*44*). The space group *P2₁/n* was determined based on systematic absences and intensity statistics. A direct methods solution was calculated, which provided most non-hydrogen atoms from the E-map. Full-matrix least-squares/difference Fourier cycles were performed, which located the remaining non-hydrogen atoms. All non-hydrogen atoms were refined with anisotropic displacement parameters. All hydrogen atoms were placed in ideal positions and refined as riding atoms with relative isotropic displacement parameters. The final full-matrix least-squares refinement converged to $R_1 = 0.0481$ and $wR_2 = 0.0920$ (F^2, all data).

2.5.3 *trans-[Rh([16]aneS₄)(H₂O)Cl)](OTf)₂* (**4**)

A crystal (approximate dimensions $0.19 \times 0.19 \times 0.07$ mm^3) was placed onto the tip of a 0.1 mm diameter glass capillary and mounted on a Rigaku AFC8S Mercury CCD diffractometer for a data collection at 153(2) K. A preliminary set of cell constants was calculated from reflections harvested from a few frames. The data collection was carried out using Mo Kα radiation (graphite monochromator). The intensity data were corrected for absorption and decay (REQAB) (*42*). Final cell constants were calculated from the *xyz* centroids of 10,120 strong reflections from the actual data collection after integration (CrystalClear) (*43*). Refer to Table 1 for additional crystal and refinement information. The structure was solved and refined using SHELXTL 6.10 (*44*). The space group *P-1* was determined based on systematic absences and intensity statistics. A direct methods solution was calculated, which provided most non-hydrogen atoms from the E-map. Full-matrix least-squares/difference Fourier cycles were performed, which located the remaining non-hydrogen atoms. All non-hydrogen atoms were refined with anisotropic displacement parameters. Positions of the water ligand hydrogen atoms were located from difference Fourier maps with the O—H distances restrained to 0.83(2) Å. All remaining hydrogen atoms were placed geometrically and treated as riding atoms with C—H lengths of 0.96 Å. The final full-matrix least-squares refinement converged to $R_1 = 0.0525$ and $wR_2 = 0.1550$ (F^2, all data).

2.5.4 *[{Pd([9]aneS₃)(Cl)}₂(pyrazine)](OTf)₂* (**6**)

A crystal (approximate dimensions $0.19 \times 0.19 \times 0.07$ mm^3) was placed onto the tip of a 0.1 mm diameter glass capillary and mounted on a Rigaku AFC8S Mercury CCD diffractometer for data collection at 158(2) K. A preliminary set of cell constants was calculated from reflections harvested from a few frames. The data collection was carried out using Mo Kα radiation (graphite monochromator). The intensity data were

corrected for absorption and decay (REQAB) (*42*). Final cell constants were calculated from the *xyz* centroids of 14,499 strong reflections from the actual data collection after integration (CrystalClear) (*43*). Refer to Table 1 for additional crystal and refinement information. The structure was solved and refined using SHELXTL 6.10 (*44*). The space group *C2/m* was determined based on systematic absences and intensity statistics. A direct methods solution was calculated, which provided most non-hydrogen atoms from the E-map. Full-matrix least-squares/difference Fourier cycles were performed, which located the remaining non-hydrogen atoms. All non-hydrogen atoms were refined with anisotropic displacement parameters. All hydrogen atoms were placed in ideal positions and refined as riding atoms with relative isotropic displacement parameters. The complex has two triflate counterions which are disordered. A reasonable disorder model could not be determined, so SQUEEZE was used in PLATON to account for the missing electron density (*45*). The final full-matrix least-squares refinement converged to $R_1 = 0.0429$ and $wR_2 = 0.1230$ (F^2, all data).

3. Results and discussion

3.1 Syntheses and NMR spectroscopy

A key goal of the research project was to explore triflic acid as an alternative to silver dechlorination for platinum group metal thiacrown complexes in preparation for their use in self-assembly reactions. However, we note that full dechlorination of the metal ion never occurred on a regular basis. Indeed, the complex [Ir([9]aneS$_3$)Cl$_3$] failed to react with triflic acid to any degree. This identical reaction works readily for amine complexes with inert d^6 metal ions such as Co(III) and Rh(III) (*36*, *37*). We believe that our synthetic results are due to the enhanced π-acidity of the thiacrown ligands, which reduces the ability of the chloride–metal bond to be broken. Since reaction stoichiometry cannot be precisely controlled due to the large excess of triflic acid, a mixture of partially dechlorinated products is observed, which complicates isolation of a single precursor complex. Accordingly, this synthetic route cannot be recommended as an improved alternative procedure to current methods based upon silver(I) salts, particularly given the hazards and difficulties posed by handling triflic acid.

We have also attempted to examine a variety of reaction conditions (solvent, temperature, silver salts, etc.) in the formation of the reported Pt/[9]aneS$_3$ molecular square and report an enhancement in its synthetic yield (*29*). Silver dechlorination of the starting reagent [Pt([9]aneS$_3$)Cl$_2$] in MeCN results in the formation of [Pt([9]aneS$_3$)(MeCN)$_2$]$^{2+}$. We further note that vigorous reaction conditions of refluxing MeCN with excess Ag(I) convert a portion of [Pt([9]aneS$_3$)(MeCN)$_2$]$^{2+}$ into the homoleptic *bis* complex, [Pt([9]aneS$_3$)$_2$]$^{2+}$ (see structural discussion below). We suggest that this is due to the high thermodynamic stability of the *bis*[9]aneS$_3$ complex and illustrates the balance between conditions favouring the kinetic vs. the thermodynamic product in the self-assembly process. Indeed, we have attempted an identical self-assembly process using the analogous [Pd([9]aneS$_3$)-Cl$_2$] complex as a precursor, but even modest heating produces a characteristic green product that is identified as [Pd([9]aneS$_3$)$_2$]$^{2+}$. The difference in reactivity between the Pt(II) and Pd(II) complexes reflects the relative kinetic stability of the two group 10 metal ions. In that regard, previous attempts to synthesise heteroleptic Ni(II) [9]aneS$_3$ complexes with diimine ligands (e.g. 2,2′-bipyridine) formed exclusively [Ni([9]aneS$_3$)$_2$]$^{2+}$(*46*). In acetonitrile, the [Pt([9]aneS$_3$)(OTf)$_2$] complex converts to a *bis* MeCN complex in acetonitrile as demonstrated by its crystal structure, and the displacement of two coordinated acetonitrile ligands by 4,4′-bipyridine facilitates square formation. In CD_3NO_2 solvent, the [Pt([9]aneS$_3$)(OTf)$_2$] complex shows bound water molecules as indicated by a downfield broad singlet in its proton NMR spectrum, presumably from residual water in the d_3-nitromethane.

The crystal structure of [{Pt([9]aneS$_3$)(bipy)}$_4$](OTf)$_8$ is unusual in that four out of the eight triflate ions are found within the square cavity, essentially filling the space. Counteranions are not typically found inside molecular squares and other self-assembled structures, but rather lie on the perimeter of the structures with solvent molecules more commonly filling the spatial voids (*1*, *47*, *48*). In order to probe this particular aspect of the Pt/[9]aneS$_3$ square, we have performed variable temperature ^{19}F NMR studies on the square in CD_3CN. We observe a single ^{19}F NMR resonance for the triflate ion, which shows no change in either its chemical shift or line width with temperature, consistent with a single invariant environment of the triflate. We, therefore, believe that the four triflate anions are not retained inside the square in solution, but rather migrate out from the cavity.

Our initial report on the [{Pt([9]aneS$_3$)(bipy)}$_4$](OTf)$_8$ square described multinuclear NMR spectra obtained in CD_3NO_2, and we have observed no change in the molecular square over a multiday period in that solvent (*29*). Dissolution of the prepared molecular square in CD_3CN shows the expected two doublets at 8.98 and 7.89 ppm for the bipy linker. However, within 20 min, a second pair of equal intensity doublets at 8.80 and 7.80 ppm begins to appear in the proton NMR spectrum, in contrast to its behaviour in nitromethane. These new peaks are not associated with the free 4,4′-bipy ligand (see Supplementary Information), and they grow in intensity until there are no further changes after a 2-week period. We hypothesize that the second pair of peaks is associated with a molecular triangle formed in equilibrium with the square, and the integral ratio of the proposed square/

triangle proton resonances at 25°C is 79/21. The appearance of a second coordination polymer is further supported by the ^{13}C NMR spectrum in CD_3CN, which also shows two symmetrical bipy environments that are not free ligand (see Supplementary Information). The distinctive [9]aneS_3 region in the ^{13}C NMR spectrum does not resolve into two separate peaks, but shows a very broad resonance, suggesting that the two [9]aneS_3 environments are close in chemical shift values. There have been several prior reports of equilibria involving molecular squares and triangles (*49–54*).[1] Efforts are currently underway in our laboratory to confirm the identity of the second component and to elucidate in more detail the equilibrium between these two species.

3.2 *Structures*

3.2.1 *Crystal structure of* $[Pt([9]aneS_3)(MeCN)_2]_2[Pt([9]aneS_3)_2](PF_6)_6$ (**2**)

The structure is not as expected, and a thermal ellipsoid perspective of the structure is shown in Figure 1. The structure consists of a solid solution of two hexafluorophosphate salts with two different complex dications. One complex dication contains a Pt(II) centre with a single [9]aneS_3 ligand and two coordinated acetonitrile molecules. The second complex dication also contains a Pt(II) centre but instead contains two coordinated [9]aneS_3 ligands. The unit cell consists of two $[Pt([9]aneS_3)(NCCH_3)_2]^{2+}$ cations, one $[Pt([9]aneS_3)_2]^{2+}$ cation and six hexafluorophosphate counterions. No solvent molecules are present. The asymmetric unit consists of one $[Pt([9]aneS_3)(MeCN)_2]^{2+}$ cation, three PF_6 anions and one-half of a $[Pt([9]aneS_3)_2]^{2+}$ cation since the Pt centre of the cation (Pt2) lies on an inversion centre at (*0.5*, *0.5*, *0.0*).

The presence of the coordinated acetonitrile in the structure importantly confirms its ability to bind to the Pt (II) in a *cis bis* fashion, which is a key factor in the self-assembly process into a molecular square. The $[Pt([9]aneS_3)(MeCN)_2]^{2+}$ cations form the anticipated elongated square pyramidal structures, which are commonly observed for heteroleptic crown thioether complexes of Pt(II) and Pd(II) (*55*, *56*). The two sulphur donors from the [9]aneS_3 macrocycle and two *cis* N donors from the MeCN ligands form the square planar array around the Pt(II). The third sulphur shows the anticipated axial interaction with the Pt to complete the square pyramidal structure and form a geometry best described as a *cis*-$[S_2N_2+S_1]$ coordination environment. The two equatorial Pt—S bond distances are 2.242(2) Å (S1) and 2.257(2) Å (S2) with the axial Pt—S distance (Pt1—S3) at 2.9963(23) Å. The Pt(II) ion is raised slightly (0.036 Å) above the mean square plane of the S_2N_2 donor set and directed towards the axial sulphur donor. The coordination plane of the four ligating atoms around the Pt(II) is quite

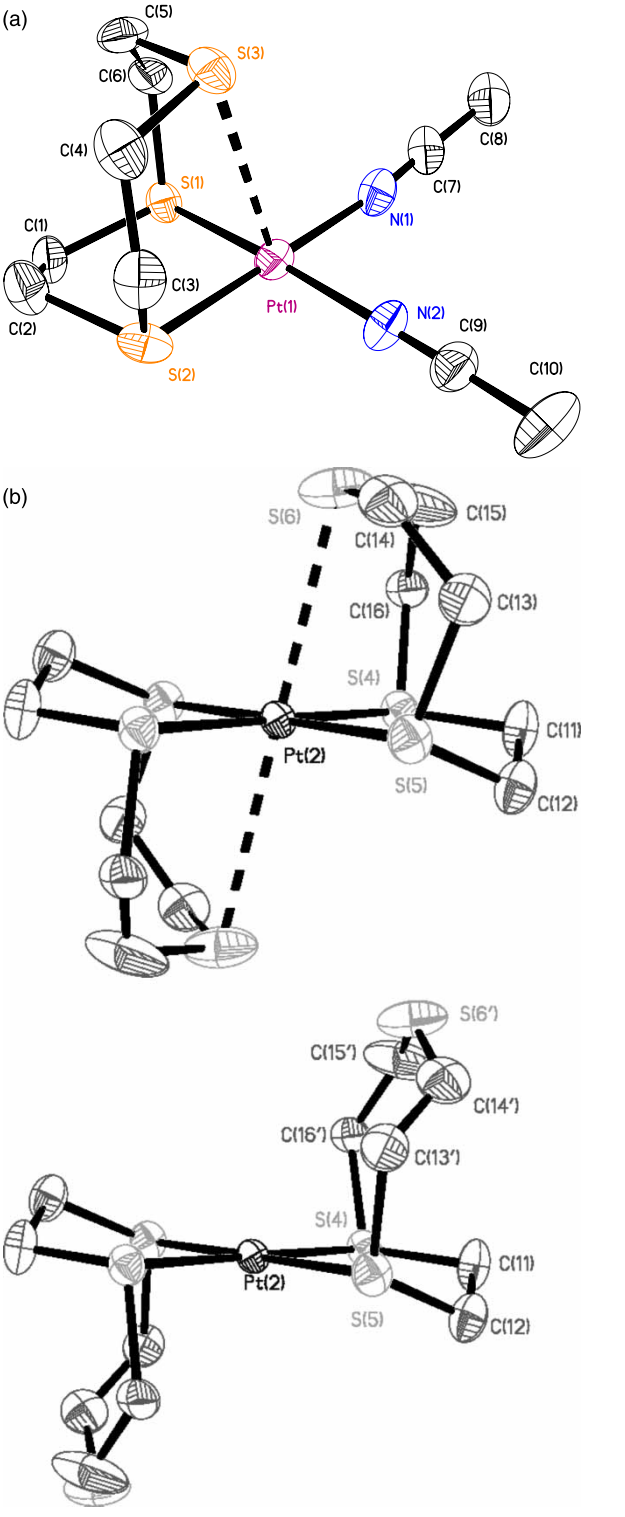

Figure 1. Thermal ellipsoid perspectives of each cation in $[Pt([9]aneS_3)(MeCN)_2]_2[Pt([9]aneS_3)_2](PF_6)_6$ (**2**). (a) $[Pt([9]aneS_3)(MeCN)_2]^{2+}$(50% probability, H atoms omitted for clarity) and (b) $[Pt([9]aneS_3)_2]^{2+}$, both the *endo* and *exo* disorder components are shown, respectively (50% probability, H atoms omitted for clarity).

planar, with a mean deviation from a least-squares plane (Pt1, S1, S1, N1 and N1) of 0.028 Å. There are over 45 crystal structures of Pt [9]aneS$_3$ complexes reported in the literature, but this is the first example involving a coordinated nitrile ligand (*57*). The Pt—N distances are 2.000(7) and 2.034(8) Å and are noticeably shorter than the Pt—N distances reported in diimine complexes of [9]aneS$_3$, such as substituted 2,2′-bipyridine and 1,10-phenanthroline ligands, which range from 2.05 to 2.08 Å (*58*, *59*). The shorter distances reflect the sp nature of the N donor in the acetonitrile as opposed to the sp^2 donor in the diimine ligands. The most interesting intermolecular feature is a relatively short approach between the coordination planes of neighbouring $[Pt([9]aneS_3)(NCCH_3)_2]^{2+}$ cations (see Supplementary Information). The closest Pt—Pt approach is 3.77 Å between Pt1 of one $[Pt([9]aneS_3)(NCCH_3)_2]^{2+}$ cation and a neighbouring $[Pt([9]aneS_3)(NCCH_3)_2]^{2+}$ cation. The distance between the least-squares planes formed by the atoms Pt1, S1, S2, N1 and N2, the analogous atoms of the neighbouring $[Pt([9]aneS_3)(NCCH_3)_2]^{2+}$ cation, is 3.66 Å. The sum of van der Waals radii for two Pt atoms is 3.44 Å, so there may be a weak Pt–Pt interaction present (*60*).

As noted, the thiacrown in the $[Pt([9]aneS_3)_2]^{2+}$ cation adopts two different conformations modelled as disorder, with both *endo* and *exo* coordinations of the Pt by the [9]aneS$_3$ ligands. In each disorder model, the $[Pt([9]aneS_3)_2]^{2+}$ cation shows both [9]aneS$_3$ ligands centrosymmetrically bound to the Pt centre with equatorial Pt—S distances at 2.288(2) and 2.303(2) Å. The all *endodentate* disorder component results in an elongated octahedral geometry (S_4+S_2 coordination) with an axial Pt—S distance of 3.0796(34) Å (Pt2—S6). This all *endodentate* [9]aneS$_3$ conformation has been commonly observed in several structural examples of $[Pt([9]aneS_3)_2]^{2+}$ cations containing a variety of anions including hexafluorophosphate, and the axial Pt—S distance is comparable to prior results (*61*, *62*). However, the all *exodentate* [9]aneS$_3$ disorder component is quite rare and has never been observed in any *bis*[9]aneS$_3$ complex for Pt(II) and Pd(II).[2] The axial Pt—S distance for the *exodentate* conformation of [9]aneS$_3$ is 4.027(13) Å (Pt2–S6′), which exceeds the van der Waals radius sum of 3.5 Å (*63*).

3.2.2 *Crystal structure of [Rh([12]aneS$_4$)Cl$_2$](PF$_6$)* (**3**)

A thermal ellipsoid perspective of the structure is shown in Figure 2. The structure shows a mononuclear complex, which consists of a Rh(III) centre bound by a tetradentate [12]aneS$_4$ ligand, two chloride ligands coordinated in a *cis* fashion and a single PF$_6$ counterion. There are no solvate molecules present, and the asymmetric unit consists of two complete monocation/monoanion pairs. The [12]aneS$_4$ is folded in an all *cis* fashion such that each chloride ligand lies *trans* to a thioether sulphur donor. The orientation for the lone pair electrons of the two equatorial sulphurs on the [12]aneS$_4$ ligand is in/out as illustrated in Scheme 2. Several research groups including ours have observed the

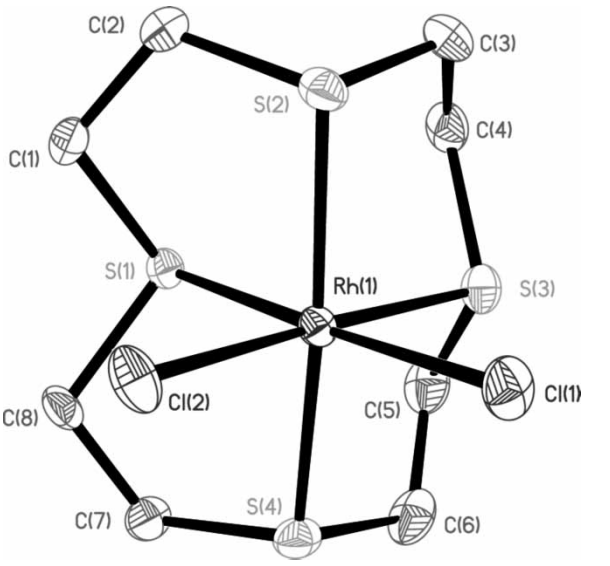

Figure 2. Thermal ellipsoid perspective of complex cation in *cis*-[Rh([12]aneS$_4$)Cl$_2$](PF$_6$) (**3**) (50% probability, H atoms omitted for clarity).

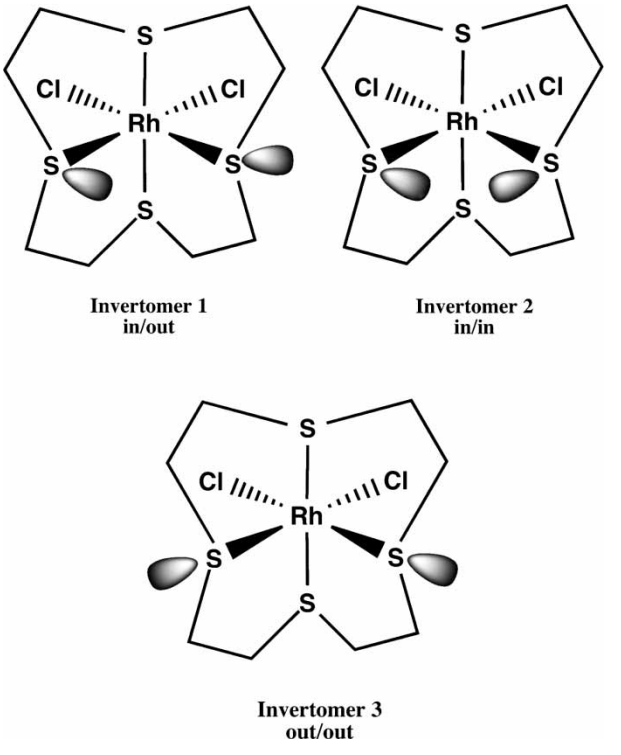

Scheme 2. Lone pair electron orientation for equatorial sulphurs in Rh/[12]aneS$_4$ complexes.

identical [12]aneS$_4$ invertomer in related Ru(II) complexes with this ligand (*64*, *65*), and the same in/out invertomer is also seen in the only other reported Rh[12]aneS$_4$ structure (*66*). Due to the different electron orientations, there is no mirror symmetry with a plane coincident with the Rh(III) centre and the two axial sulphurs. However, there is nearly mirror symmetry with respect to the equatorial plane. That is, the ethylene straps of the [12]aneS$_4$ ligand have essentially identical but not crystallographically related conformations. The four-line ^{13}C NMR for the coordinated [12]aneS$_4$ ligand is consistent with the in/out orientation of lone pair electrons on the equatorial sulphurs, again similar to observations with the isoelectronic Ru(II) species (*64*, *65*). Due to the *trans* influence of the chloride ligands, the Rh—S bond distances for the equatorial sulphurs are about 0.04–0.08 Å shorter than the axial Rh—S bonds. Also, the S_{axial}—Rh—S_{axial} angles are considerably less than 180° (S(8)—Rh(2)—S(6) 170.66(5)°, S(2)—Rh(1)—S(4) 170.74(5)°) due to the steric constraints imposed by the folding of the small 12-membered macrocyclic ring onto the relatively small trivalent Rh ion. The Cl—Rh—S_{eq} angles are distinctive in that the angles involving the sulphur with its lone pair electrons pointing towards the other equatorial sulphur are greater than 90° (S(1)—Rh(1)—Cl(2) = 92.66(4)°, S(7)—Rh(2)—Cl(3) = 92.55(4)°), while the angles involving the sulphur with the lone pair pointing away from the other equatorial sulphur are less than 90° (S(3)—Rh(1)—Cl(1) = 86.26(5)°, S(5)—Rh(2)—Cl(4) = 85.69(5)°).

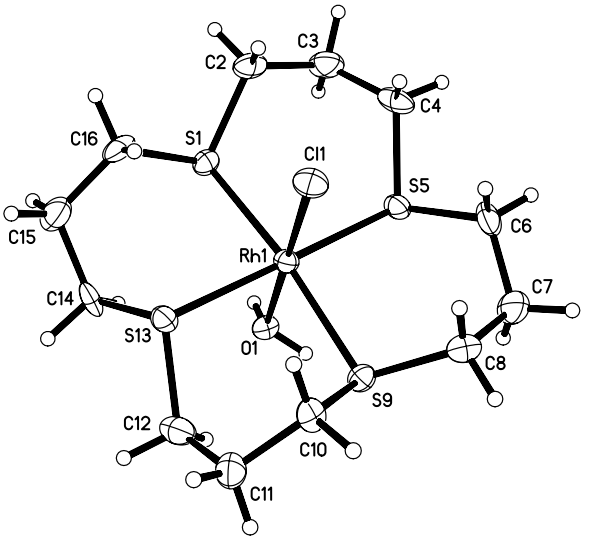

Figure 3. Thermal ellipsoid perspective of complex cation in *trans*-[Rh([16]aneS$_4$)(H$_2$O)Cl](OTf)$_2$ (**4**) (50% probability).

3.2.3 *Crystal structure of trans-[Rh([16]aneS$_4$)(H$_2$O)Cl](OTf)$_2$ (**4**)*

A thermal ellipsoid perspective of the structure is shown in Figure 3. In the complex, the Rh(III) centre is bound to the [16]aneS$_4$ macrocycle with a *trans* water and a chloride ligand. Two triflate counterions are also present, but there are no uncoordinated solvent molecules. Importantly, the structure reveals that full dechlorination of the Rh(III) via triflic acid has not occurred. Of particular interest is the comparison of this structure with the previously reported related *trans*-[Rh([16]aneS$_4$)Cl$_2$](PF$_6$) (*39*), the only other Rh[16]aneS$_4$ complex in the Cambridge Structural Database (*57*). In our case, the stronger field water ligand, which is now *trans* to the remaining chloride, results in significant electronic changes on the Rh(III) centre and corresponding structural changes within the Rh coordination environment. The most noteworthy is the reduction by about 0.04 Å of the Rh—Cl bond distance (2.301(2) Å) compared to the Rh—Cl bond length (2.3391(22) Å) in the dichloro complex (Table 2). Similarly, all Rh—S bonds are also affected. They average 2.3483(2) Å in the dichloro complex, but lengthen to an average of 2.356(2) Å in our

Table 2. Selected lengths (Å)[a] for [Pt([9]aneS$_3$)(MeCN)$_2$]$_2$[Pt([9]aneS$_3$)$_2$](PF$_6$)$_6$ (**2**), [Rh([12]aneS$_4$)Cl$_2$](PF$_6$) (**3**), *trans*-[Rh([16]aneS$_4$)(H$_2$O)Cl)](OTf)$_2$ (**4**) and [{Pd([9]aneS$_3$)(Cl)}$_2$(pyrazine)](OTf)$_2$ (**6**).

	2		**3**		**4**	**6**
Bond lengths						
M–S[b]	2.242 (2)[c]	2.288 (2)[c]	2.2684 (12)[c]	2.2711 (12)[c]	2.3453 (18)	2.2557 (12)
	2.257 (2)	2.303 (2)	2.2874 (12)	2.2833 (12)	2.3544 (18)	2.2804 (12)
	3.090 (2)		2.3291 (13)	2.3183 (14)	2.3546 (18)	2.8961 (13)
			2.3389 (14)	2.3449 (14)	2.3680 (18)	
M–Cl[b]	NA		2.3685 (12)	2.3702 (12)	2.3012 (18)	2.3397 (12)
			2.3697 (12)	2.3741 (12)		
M–N	2.000 (7)		NA		NA	2.090 (4)
	2.034 (8)					
Rh–O	NA		NA		2.101 (4)	NA

[a] Estimated standard deviations are given in parentheses.
[b] M = Pt, Rh or Pd.
[c] Two crystallographically independent cations are present.

structure. Furthermore, there is virtually no variation in length among the four Rh—S bonds in the dichloro structure, but a large variation in distances (2.368(2), 2.354(2), 2.355(2), 2.435(2) Å) for the aqua/chloro complex. As a consequence of these alterations in the rhodium–sulphur distances, the [16]aneS$_4$ macrocycle adopts a different conformation around the rhodium. Both structures show the six-membered chelate rings of the thiacrown displaying two chair conformations and two twist-boat conformations. However, in the dichloro structure, the two chair conformations are *trans*, whereas they are *cis* in the current structure. The change in the conformation for the [16]aneS$_4$ macrocycle along with two different *trans* monodentate ligands results in a more complex ^{13}C NMR spectrum in contrast to the simple four-line ^{13}C NMR spectrum (two lines for each conformation) observed for the dichloro complex (*39*). In MeCN solvent, the water is readily replaced by acetonitrile, but NMR studies suggest that in anhydrous non-coordinating solvents such as nitromethane, the coordination site is filled by a triflate anion since two different triflate environments are observed in both the ^{13}C and ^{19}F NMR spectra of the complex. In our current structure, the longest Rh—S bond (Rh—S13; 2.368(2) Å) lies between the two *cis* twist-boat conformations, while the shortest bond (Rh—S5; 2.343(2) Å) lies between the two chair conformations. The change in conformation can also be seen in the *trans* S—Rh—S angles. In the dichloro complex, both are 180° due to symmetry restrictions, but in the current structure, the larger S—Rh—S angle (S5—Rh—S13; 178.81(6)°) is found along the pseudo-mirror plane that bisects both the chair and twist-boat conformations. The smaller S—Rh—S angle (S9—Rh—S1; 172.56(6)°) divides one conformation from the other. Interestingly, the related Ru(II) structure of [Ru([16]aneS$_4$)(H$_2$O)(dmso)](CF$_3$SO$_3$)$_2$ recently reported by the Alessio group shows all four six-membered chelate rings of the [16]aneS$_4$ exclusively in a chair conformation (*30*).

3.2.4 *Crystal structure of [{Pd([9]aneS$_3$)(Cl)}$_2$(pyrazine)](OTf)$_2$ (**6**)*

A thermal ellipsoid perspective of the cation's structure is shown in Figure 4. The complex cation is formed by a bidentate, bridging pyrazine ligand linking two [Pd([9]aneS$_3$)Cl]$^+$ moieties together in a binuclear fashion. Two triflates are present as counterions, but there are no solvent molecules present. The two halves of the binuclear complex cation are related by mirror symmetry. Each Pd(II) centre is surrounded by an elongated square pyramidal environment, formed by three sulphurs from the [9]aneS$_3$ ligand, a chloride and a nitrogen donor of the pyrazine, and the two chloride ligands lie in a *cis* orientation. The complex environment around the Pd is then best described as *cis*-[S$_2$NCl + S$_1$] geometry. The Pd(II) lies 0.057 Å above the mean least-squares plane defined by the S$_2$NCl donor set. The *cis* stereoisomer is atypical in that virtually all other pyrazine-bridged binuclear complexes of this type show *trans* stereochemistry of the chloride donors (*3*, *67*). The other exception is the complex [{Pt(NH$_3$)$_2$(Cl)}$_2$(pz)]$^{2+}$ whose structure was reported by the Lippert group as a perchlorate salt (*68*) and the Reedjik group as a nitrate salt (*69*). Interestingly, Reedjik and co-workers have reported the use of these types of binuclear pyrazine-bridged Pt(II) complexes as being able to overcome cross-resistance to *cis*-platin (*69*). Note that a *cis* stereochemistry will be required for self-assembly into a molecular square or related structure, and the reported structure represents two corners and one side towards the formation of a square.

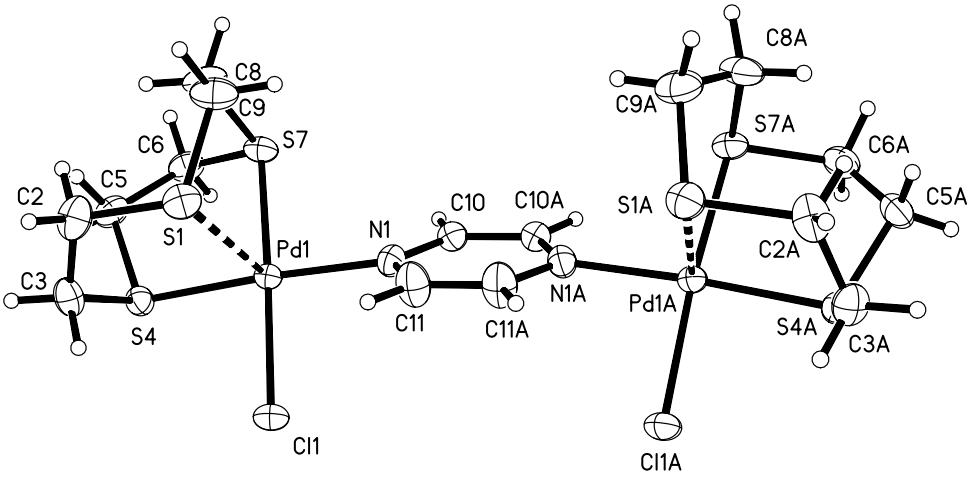

Figure 4. Thermal ellipsoid perspective of complex cation in [{Pd([9]aneS$_3$)(Cl)}$_2$(pyrazine)](OTf)$_2$ (**6**) (50% probability).

In the square planar array around a single Pd(II) centre, the stronger *trans*-directing chloro ligand results in a shorter Pt—S bond *trans* to it (2.2557(12) Å) as opposed to the one *trans* to the pyrazine nitrogen (2.2804(12) Å). As seen in virtually all Pt(II) and Pd(II) [9]aneS$_3$ complexes, there is a longer Pd–S$_{axial}$ interaction (2.8961(13) Å) with the third sulphur in the [9]aneS$_3$ macrocycle, similar to that observed in compound **2**. The mean least-squares plane of the pyrazine ring is turned at a 52.0° angle relative to the mean least-squares plane defined by the square planar donor set. The value falls in the mid-range of related pyrazine-bridged structures whose angles range from 45.6° to 63.8° (*67*). For comparison, we also include the synthesis and characterisation of the related binuclear Pt(II) [9]aneS$_3$ complex with a 4,4′-bipyridine bridge, [{Pt([9]aneS$_3$)(Cl)}$_2$(bipy)](PF$_6$). Unfortunately, we have not been able to obtain a crystal structure on the compound to determine the stereochemistry around the Pt centre. However, we note that we obtain a single ^{195}Pt NMR resonance as well as a single ^{13}C NMR resonance in the [9]aneS$_3$ region, suggesting there is only one Pt complex in solution.

The dihedral angle for the Pd—N—N—Pd unit is nearly linear at 0.028°, but the Pd–centroid(pyrazine)–Pd angle is 170.8°, significantly distorted for the ideal value of 180°. The 'bowing' of the pyrazine ring can clearly be seen in the structure, and similar distortions have been observed in another pyrazine-linked triangles, all of which show a comparable bowing (165–171° angles) to relieve strain in the triangular shape (*70–72*). Interestingly, the related molecular square with pyrazine linkers reported by Fujita shows little distortion (Pt–centroid(pyz)–Pt angle = 177.8°) consistent with less strain in the molecular square (*73*). The angle of Pd–centroid(pyz)–Pd is identical in the two dimeric chains, but the bowing occurs in opposite directions and away from the centre of the two chains. The extended structure is remarkable in that it consists of linear dimeric chains running parallel to the *b*-axis of the crystal. The cationic complexes involved in a dimer are shown in Figure 5, with perpendicular perspectives parallel to two of the crystallographic axes. The chloride ligands in the complexes in one of the chains lie *anti* relative to the chloride ligands in the second set of chains within the dimers. The dimers are held together by weak Pd–Pd electronic interactions (distance = 3.68 Å), which are facilitated by the axial sulphur of the [9]aneS$_3$ ligand. Note that the Pd–Pd interaction between the chains of the dimers is *trans* to the axial sulphur. Our group has reported a similar metal–metal dative interaction (Pt(II) → Ag(I) in that case) for a Pt[9]aneS$_3$ complex with the ligand phenylpyridine (*74*). As a consequence of the Pd–Pd interactions, the Pd—S$_{axial}$ distance is shorter (by over 0.1 Å) than expected for a Pd(II) [9]aneS$_3$ complex with a [S$_2$NCl + S$_1$] environment (*56*, *75*).[3] The formation of the dimeric chains is further facilitated by intermolecular π–π interactions involving the pyrazine rings between the two chains. In the chains, the pyrazine rings stack face-to-face in a parallel fashion with a centroid(pyz)—centroid(pyz) distance of 3.58 Å.

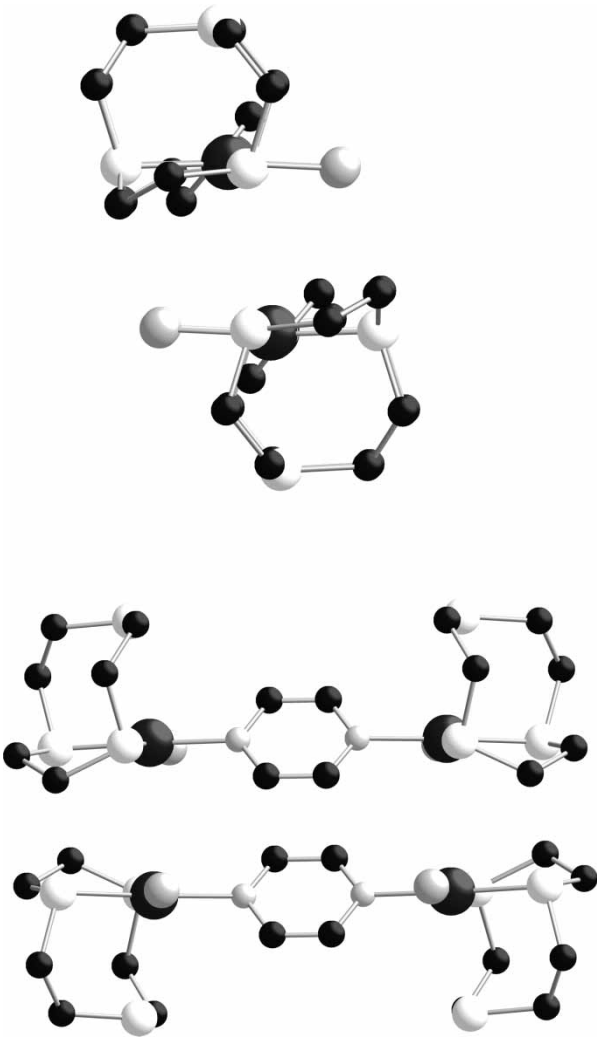

Figure 5. View of two chains of dimeric complex cations in [{Pd([9]aneS$_3$)(Cl)}$_2$(pyrazine)](OTf)$_2$ (**6**). Top view is along the *b*-axis, bottom along the *a*-axis. H atoms omitted for clarity.

4. Conclusions and summary

Transition metal thiacrown complexes containing chloride ligands fail to become fully dechlorinated with triflic acid, making the synthetic method unreliable for the preparation of precursors in transition-mediated self-assembly processes. Reaction of [Pt([9]aneS$_3$)Cl$_2$] with excess AgPF$_6$ in refluxing MeCN forms a solid-state solution containing two complex cations with exclusive hexafluorophosphate counterions. One of these, [Pt([9]aneS$_3$)(MeCN)$_2$]$^{2+}$, shows coordinated acetonitrile ligands from the solvent and forms the expected elongated square pyramidal structure. The second, [Pt([9]aneS$_3$)$_2$]$^{2+}$, shows

disorder between an all *endo* and a rare all *exo* conformation for the two [9]aneS$_3$ ligands. The structure of [Rh([12]aneS$_4$)Cl$_2$] demonstrates *cis* chloro ligands with asymmetric binding of the two equatorial sulphur donors. The complex *trans*-[Rh([16]aneS$_4$)(H$_2$O)(Cl)](OTf)$_2$ exhibits adjacent rather than alternating chair and twist-boat conformations. The structure of [{Pd([9]aneS$_3$)(Cl)}$_2$(pyrazine)](OTf)$_2$ shows a pyrazine ligand bridging two [Pd([9]aneS$_3$)Cl]$^+$ moieties with *cis* stereochemistry of the two chloro ligands. The extended structure of the complex consists of chains of dimers running parallel to the *b*-axis of the crystal. Measurements using ^{19}F NMR spectroscopy on the previously reported molecular square, [{Pt([9]aneS$_3$)(bipy)}$_4$](OTf)$_8$, show that the triflate ions migrate out of the square cavity in solution, in contrast to its solid-state solution.

Supplementary Information

CCDC nos 737493–737496 contains the supplementary crystallographic data for compounds **2**–**4** and **6**, respectively. Supplementary Information is also available online containing NMR spectra, synthetic procedures and structural diagrams.

Acknowledgements

We thank Ketankumar Patel for his preparation of compound **5**. Acknowledgements are made to the following organisations for their generous support of this research: the donors of the American Chemical Society Petroleum Research Fund; the Research Corporation; the Grote Chemistry Fund at the University of Tennessee at Chattanooga; the National Science Foundation RUI Program.

Notes

1. From (*49*). Fujita and co-workers reported exclusive observation of a molecular square when using Pt(II)/ethylenediamine corners. However, they observe *both* a square and a triangle when 2,2-bipyridine replaces ethylenediamine as we obtain here. We note that [9]aneS$_3$, similar to 2,2′-bipyridine, is a π-acceptor ligand. A recent report from the Besenyei group (*52*) describes a 94/6 square/triangle ratio following up the work on the Fujita square.
2. *Exodentate* [9]aneS$_3$ coordination is also rare in heteroleptic Pt(II) or Pd(II) complexes with only three confirmed examples that have been crystallographically characterised (total of 71 structures in *Cambridge Structural Database v 5.30*, May, 2009). The three examples are: (1) [Pt([9]aneS$_3$)$_2$](PF$_6$)$_2$, one *endo*, one *exo* conformation on each Pt, two whole complex cations per asymmetric unit, Pt—S$_{exo}$ = 4.04 and 4.17 Å; *Chem. Commun.* **1987**, 118–120; CCDC code FAGSAH. (2) [Pt([9]aneS$_3$)](bq)(PF$_6$), bq = benzoquinoline; *exodentate* component of [9]aneS$_3$ disorder, Pt—S$_{exo}$ = 4.12 Å; see (*71*); CCDC code VIYYAE. (3) [Pt([9]aneS$_3$)(Ph)$_2$]; exclusively *exodentate,* Pt—S$_{exo}$ = 4.10 Å; *Inorg. Chem.* **1993,** *32*, 1951–1958, CCDC code PITTOB.
3. The presence of a chloro ligand in the Pt(II) or Pd(II) [9]aneS$_3$ complex always results in an elongation of the axial sulphur distance by 0.4–0.5 Å [see (*75*)]. However, the Pd—S axial distances here are virtually identical to those observed in the bipy complex (2.81 Å) and even shorter than in the phen complex [2.95 Å, see (*56*) as well as (*76*)].

References

(1) Fujita, M.; Yazaki, J.; Ogura, K. *J. Am. Chem. Soc.* **1990**, *112*, 5645–5647.
(2) Stang, P.J.; Cao, D.H. *J. Am. Chem. Soc.* **1994**, *116*, 4981–4982.
(3) Balzani, V.; Credi, A.; Raymo, F.M.; Stoddart, J.F. *Angew. Chem., Int. Ed. Engl.* **2000**, *39*, 3348–3391.
(4) Sauvage, J.-P. *Acc. Chem. Res.* **1998**, *31*, 611–619.
(5) Balzani, V.; Gomez-Lopez, M.; Stoddard, J.F. *Acc. Chem. Res.* **1998**, *31*, 405–414.
(6) Rosi, N.; Eckert, J.; Eddaoudi, M.; Vodak, D.T.; Kim, J.; O'Keeffe, M.; Yaghi, O.M. *Science* **2003**, *300*, 1127–1129.
(7) Eddaoudi, M.; Kim, J.; Rosi, N.; Vodak, D.T.; Wachter, J.; O'Keeffe, M.; Yaghi, O.M. *Science* **2002**, *295*, 469–472.
(8) Fletcher, A.J.; Cussen, E.J.; Prior, T.J.; Risseinsky, M.J.; Kepert, C.J.; Thomas, K.M. *J. Am. Chem. Soc.* **2001**, *123*, 10001–10011.
(9) Kondo, M.; Yoshitomi, T.; Seki, K.; Matsuzaka, H.; Kitagawa, S. *Angew. Chem., Int. Ed. Engl.* **1997**, *36*, 1725–1727.
(10) Chae, H.K.; Siberio-Perez, D.Y.; Kim, J.; Go, Y.; Eddaoudi, M.; Matzger, A.J.; O'Keeffe, M.; Yaghi, O.M. *Nature* **2004**, *427*, 523–527.
(11) Khobystov, A.N.; Brett, M.T.; Blake, A.J.; Champness, N.R.; Gill, P.M.; O'Neill, D.P.; Teat, S.J.; Wilson, C.; Schröder, M. *J. Am. Chem. Soc.* **2003**, *125*, 6753–6761.
(12) Fiedler, D.; Leung, D.H.; Bergman, R.G.; Raymond, K.N. *Acc. Chem. Res.* **2005**, *38*, 351–360.
(13) Fiedler, D.; Leung, D.H.; Bergman, R.G.; Raymond, K.N. *Strem Chemiker* **2005**, *12*, 4–11.
(14) Zhao, H.; Heintz, R.A.; Ouyang, X.; Dunbar, K.R.; Campana, C.F.; Rogers, R.D. *Chem. Mater.* **1999**, *11*, 736–746.
(15) Caulder, D.L.; Raymond, K.N. *Acc. Chem. Res.* **1999**, *32*, 975–982.
(16) Hill, R.J.; Long, D.-L.; Champness, N.R.; Hubberstey, P.; Schröder, M. *Acc. Chem. Res.* **2005**, *38*, 337–350.
(17) Belanger, S.; Keefe, M.H.; Welch, J.L.; Hupp, J.T. *Coord. Chem. Rev.* **1999**, *38*, 2222–2224.
(18) Fujita, M.; Ogura, K. *Coord. Chem. Rev.* **1996**, *148*, 249–264.
(19) Cotton, F.A.; Lin, C.; Murillo, C.A. *Acc. Chem. Res.* **2001**, *34*, 759–771.
(20) Leininger, S.; Olenyuk, B.; Stang, P. *Chem. Rev.* **2000**, *11*, 853–908.
(21) Fujita, M. *Acc. Chem. Res.* **1999**, *32*, 53–61.
(22) Seidel, S.R.; Stang, P.J. *Acc. Chem. Res.* **2002**, *35*, 972–983.
(23) Navarro, J.A.R.; Lippert, B. *Coord. Chem. Rev.* **2001**, *222*, 219–250.
(24) Holliday, B.J.; Mirkin, C.A. *Angew. Chem., Int. Ed.* **2001**, *40*, 2022–2043.
(25) Sun, S.-S.; Lees, A.J. *Coord. Chem. Rev.* **2002**, *230*, 171–192.
(26) Zangrando, E.; Casanova, M.; Alessio, E. *Chem. Rev.* **2008**, *108*, 4979–5013.
(27) Berben, L.A.; Faia, M.C.; Crawford, N.R.M.; Long, J. *Inorg. Chem.* **2006**, *45*, 6378–6386.

(28) Lau, V.C.; Berben, L.A.; Long, J.R. *J. Am. Chem. Soc.* **2002**, *124*, 9042–9043.
(29) Janzen, D.E.; Patel, K.N.; VanDerveer, D.G.; Grant, G.J. *Chem. Commun.* **2006**, 3540–3542.
(30) Zangrando, E.; Kulisic, N.; Ravalico, F.; Bratsos, I.; Jender, S.; Casanova, M.; Alessio, E. *Inorg. Chim. Acta* **2009**, *362*, 820–832.
(31) Shan, N.; Ingram, J.D.; Easun, T.L.; Vickers, S.J.; Adams, H.; Ward, M.D.; Thomas, J.A. *Dalton Trans.* **2006**, 2900–2906.
(32) Cooper, S.R.; Rawle, S.C.; Yagbasan, R.; Watkin, D.J. *J. Am. Chem. Soc.* **1991**, *113*, 1600–1604.
(33) Blake, A.J.; Gould, R.O.; Holder, A.J.; Hyde, T.I.; Schröder, M. *J. Chem. Soc., Dalton Trans.* **1988**, 1861–1865.
(34) Blake, A.J.; Holder, A.J.; Hyde, T.I.; Roberts, Y.V.; Lavery, A.J.; Schröder, M. *J. Organometal. Chem.* **1987**, *323*, 261–270.
(35) Grant, G.J.; Sanders, K.A.; Setzer, W.N.; VanDerveer, D.G. *Inorg. Chem.* **1991**, *30*, 4053–4056.
(36) Dixon, N.E.; Lawrance, G.A.; Lay, P.A.; Sargeson, A.M.; Taube, H. *Inorganic Syntheses* **1990**, *28*, 243: Wiley, New York.
(37) Dixon, N.E.; Jackson, W.G.; Lancaster, M.J.; Lawrance, G.A.; Sargeson, A.M. *Inorg. Chem.* **1981**, *20*, 470–476.
(38) Grant, G.J. *Inorganic Syntheses*, **2009**, in review.
(39) Blake, A.J.; Reid, G.; Schröder, M. *J. Chem. Soc., Dalton Trans.* **1989**, 1675–1680.
(40) Timonen, S.; Pakkanen, T.T.; Pakkanen, T.A. *J. Mol. Catal.* **1996**, *111*, 267–272.
(41) Pregosin, P.S. In *Transition Metal Nuclear Magnetic Resonance*; Pregosin, P.S., Ed.; Elsevier: New York, 1991, p 251, and references cited therein.
(42) Jacobson, R. *REQAB*, Version 1.1; Molecular Structure Corporation, The Woodlands, Texas, USA, 1998.
(43) Molecular Structure Corporation and Rigaku, CrystalClear MSC, The Woodlands: TX, USA, and Rigaku Corporation, Tokyo, Japan, 2006.
(44) Sheldrick, G.M. *Acta Cryst.* **2008**, *A64*, 112. SHELXTL. Version 6.10.
(45) Spek, A.L. PLATON, A Multipurpose Crystallographic Tool, Utrecth University: Utrecht, The Netherlands, 2008.
(46) Blake, A.J.; Gould, R.O.; Halcrow, M.A.; Schröder, M. *J. Chem. Soc., Dalton Trans.* **1993**, 2909–2920.
(47) Yamashita, K.-I.; Kawano, M.; Fujita, M. *Chem. Commun.* **2007**, 4102–4103.
(48) Fujita, M.; Nagao, S.; Iida, M.; Ogati, K.; Ogura, K. *J. Am. Chem. Soc.* **1993**, *115*, 1574–1576.
(49) Fujita, M.; Sasaki, O.; Mitsuhasi, T.; Fujita, T.; Yazaki, J.; Yamaguchi, K.; Ogura, K. *Chem. Commun.* **1996**, 1535–1536.
(50) Lee, S.B.; Hwang, S.; Chung, D.S.; Yun, H.; Hong, J.-I. *Tet. Lett.* **1998**, *39*, 873–876.
(51) Cohen, Y.; Avran, L.; Frish, L. *Angew. Chem., Int. Ed.* **2005**, *44*, 520–554.
(52) Holló-Sitkei; Tárkányi, G.; Párkányi, L.; Megye, T.; Besenyei, G. *Eur. J. Inorg. Chem.* **2008**, 1573–1583.
(53) Cotton, F.A.; Murillo, C.A.; Yu, R. *Dalton Trans.* **2006**, 3900–3905.
(54) Ferrer, M.; Gutiérrez, A.; Mounir, M.; Rossell, O.; Riuz, E.; Rang, A.; Engeser, M. *Inorg. Chem.* **2007**, *46*, 3395–3406.
(55) Janzen, D.E.; VanDerveer, D.G.; Mehne, L.F.; da Dilva Fihlo, A.A.; Bredas, J.-L.; Grant, G.J. *Dalton Trans.* **2008**, 1872–1882.
(56) Blake, A.J.; Roberts, Y.V.; Schröder, M. *J. Chem. Soc., Dalton Trans.* **1996**, 1885–1985.
(57) *Cambridge Structural Database v 5.30*, Cambridge Crystallographic Data Centre, 12 Union Road, Cambridge CB2 1EZ, UK, May, 2009.
(58) Grant, G.J.; Patel, K.N.; Grant Helm, M.L.; Mehne, L.F.; Klinger, D.W.; VanDerveer, D.G. *Polyhedron* **2004**, *23*, 1361–1369.
(59) Green, T.W.; Liberman, R.; Mitchell, N.; Krause Bauer, J.A.; Connick, W.B. *Inorg. Chem.* **2005**, *44*, 1955–1956.
(60) Bondi, A. *J. Phys. Chem.* **1964**, *68*, 441–451.
(61) Grant, G.J.; Chen, W.; Goforth, A.M.; Baucom, C.L.; Patel, K.; Repovic, P.; VanDerveer, D.G.; Pennington, W.T. *Eur. J. Inorg. Chem.* **2005**, 479–485.
(62) Blake, A.J.; Gould, R.O.; Holder, A.J.; Hyde, T.I.; Lavery, A.J.; Odulate, M.O.; Schröder, M. *J. Chem. Soc., Chem. Commun.* **1987**, 118–120.
(63) Huheey, J.E.; Keiter, E.A.; Keiter, R.L. *Inorganic Chemistry*; 4th ed.; Harper Collins: New York, 1993; p 292.
(64) Janzen, D.E.; Chen, W.; VanDerveer, D.G.; Mehne, L.F.; Grant, G.J. *Inorg. Chem. Commun.* **2006**, *9*, 992–995.
(65) Santos, T.M.; Goodfellow, B.J.; Madureira, J.; de Jesus, J.P.; Félix, V.; Drew, M.G.B. *New J. Chem.* **1999**, *23*, 1015–1025.
(66) Krotz, A.H.; Kuo, L.Y.; Shields, T.P.; Barton, J.K. *Inorg. Chem.* **1993**, *115*, 5693–5974, The complex is $[(Rh([12]aneS_4)(9,10\text{-phenanthrenequinonediimine})]Br_3 \cdot 3H_2O$ (CCDC code LEFGEI).
(67) For examples of *trans* stereoisomers in pyrazine-bridged structures, see: Iengo, E.; Mestroni, G.; Calligaros, M. Alessio, E. *J. Chem. Soc., Dalton Trans.* **1999,** 3361–3371; Priqueles, J.R.L.; Rocho, F.D. *Inorg. Chim. Acta* **2004,** *357*, 2167–2175; Adams, H.; Costa, P.J.; Newell, M.; Vickers, S.J.; Ward, M.D.; Felix, V.; Thomas, J.A. *Inorg. Chem.* **2008,** *24*, 11633–11644; Halesha, R.; Reddy, G.K.N.; Rao, S.P.S.; Manoker, H. *J. Organometall. Chem.* **1983,** *252*, 231–241; Srivastava, R.S.; Fronczek, F.R.; Romero, L.M. *Inorg. Chim. Acta* **2004,** *357*, 2410–2414; Moreno, M.A.; Haukka, M.; Kallian, M.; Pakkanen, T.A. *Appl. Organometall. Chem.* **2006,** *20*, 51–54; Coe, B.J.; Meyer, T.J.; White, P.S. *Inorg. Chem.* **1995,** *34*, 593–602; Skarzynska, A.; Siczak, M. *Polyhedron*, **2008,** *27*, 1930–1936.
(68) Willerman, M.; Mulcahy, C.; Sigel, R.K.O.; Cerdá Freisinger, E.; Miguel, P.J.S.; Roitzsch, M.; Lippert, B. *Inorg. Chem.* **2006**, *45*, 2093–2099.
(69) Komeda, S.; Kalayda, G.V.; Lutz, M.; Spek, A.L.; Yamanaka, Y.; Sato, T.; Chikuma, M.; Reedijk, J. *J. Med. Chem.* **2003**, *46*, 1210–1219.
(70) Schweiger, M.; Seidel, S.R.; Arif, A.M.; Stang, P.J. *Angew Chem., Int. Ed.* **2001**, *40*, 3467–3469.
(71) Yu, X.-Y.; Maekawa, M.; Kondo, M.; Kitagawa, S.; Jin, G.-X. *Chem. Lett.* **2001**, 168–169.
(72) Derossi, S.; Casanova, M.; Iengo, E.; Zangrando, E.; Stener, M.; Alessio, E. *Inorg. Chem.* **2007**, *46*, 11243–11247.
(73) Kumaza, K.; Biradha, K.; Kusukawa, T.; Okana, T.; Fujita, M. *Angew. Chem., Int. Ed.* **2003**, *42*, 3909–3913.
(74) Janzen, D.E.; VanDerveer, D.G.; Mehne, L.F.; da Dilva Fihlo, A.A.; Bredas, J.-L.; Grant, G.J. *J. Chem. Soc., Dalton Trans.* **2008**, 1872–1882.
(75) Grant, G.J.; Benefield, D.E.; VanDerveer, D.G. *Dalton Trans.* **2009**, DOI: 10.1039/B909875E.
(76) Nikol, H.; Hans-Beat Bürgi; Hardcastle, K.I.; Gray, H.B. *Inorg. Chem.* **1995**, *34*, 6319–6322.